University of Mississippi

eGrove

10-1-2020

Electric field change and VHF waveforms of Positive Narrow Bipolar Events in Mississippi thunderstorms

Sampath Bandara
University of Mississippi

Thomas Marshall
University of Mississippi

Sumedhe Karunarathne
University of Mississippi

Maribeth Stolzenburg
University of Mississippi

Follow this and additional works at: https://egrove.olemiss.edu/physics_facpubs

ELSEVIER

Electric field change and VHF waveforms of Positive Narrow Bipolar Events in Mississippi thunderstorms

Sampath Bandara, Thomas Marshall*, Sumedhe Karunarathne[1], Maribeth Stolzenburg

Department of Physics & Astronomy, University of Mississippi, University, MS 38677, USA

ARTICLE INFO

ABSTRACT

Positive Narrow Bipolar Events (+NBEs) in Mississippi thunderstorms were studied using fast antennas (FA, bandwidth 16 Hz - 2.6 MHz) and VHF antennas (Log-RF, bandwidth 186–192 MHz). The waveform characteristics of 201 positive NBEs were determined using both sensors. The +NBEs were classified in two ways: by FA waveform into Types A-D and by +NBE occurrence relative to other lightning events into three groups called Isolated, Not-Isolated, and INBE. (An INBE initiates an intracloud flash.) The FA waveform properties of 188 positive NBEs were mainly in reasonable agreement with previous studies. The VHF waveform properties of +NBEs have not been studied previously. The VHF powers of 201 positive NBE ranged from 0.1–88.4 kW with an average value of 7.8 kW. Types C and D positive NBEs tended to be more energetic (average VHF powers of 9.2 and 13.2 kW) than Types A and B (average powers of 1.9 and 4.0 kW). The INBE group of +NBEs had a larger range of VHF powers (0.2–88.4 kW) than the combined power range of the Not-Isolated and Isolated groups (0.1–26.7 kW). The INBE group also had a larger average peak power (9.9 kW) than the Not-Isolated and Isolated Groups (4.0 and 8.7 kW, respectively). However, 53% of INBEs had peak VHF power < 5 kW, so an INBE does not require a large power to initiate an intracloud flash. For 90% of the 201 positive NBEs the magnitude of the time difference between the FA peak amplitude and the Log-RF peak power was ≤2 μs, but the FA peak amplitude showed almost no correlation with the Log-RF peak power.

1. Introduction

A narrow bipolar event (NBE) is a short, powerful lightning discharge as was first reported by Le Vine (1980). NBEs are also known as compact intracloud discharges (CIDs) or narrow bipolar pulses (NBPs). Using an electric field change ("*E*-change") sensor with a bandwidth of 500 Hz – 2 MHz, Le Vine (1980) characterized NBEs as having a bipolar waveform with a short duration (~20 μs). Le Vine's E-change sensor was triggered by one of three narrow-band (300 kHz) radio detectors with frequencies of 3, 139, or 295 MHz (i.e., in the HF and VHF radio bands). When the HF/VHF trigger threshold was set at a sufficiently high level, Le Vine (1980) recorded only NBEs from thunderstorms and thereby determined that NBEs are the "sources of the strongest radio frequency radiation from lightning."

Willett et al. (1989) studied 24 NBEs and found that the NBE bipolar E-change waveform could be either positive or negative. Using the physics convention of electric field polarity, Willett et al. (1989) defined positive and negative NBEs based on the polarity of the initial half cycle of the bipolar waveform. According to Karunarathne et al. (2015),

"in this convention and for sensors beyond the reversal distance, positive NBPs [NBEs] can be produced by negative charges moving upward (leaving positive charges along the path) and/or by positive charges moving downward (leaving negative charges along the path)."

Using E-change sensors similar to the one used by Le Vine (1980), NBEs have been extensively studied (e.g., Medelius et al., 1991; Willett et al., 1989; Smith et al., 1999; Smith et al., 2004; Hamlin et al., 2007; Ahmad et al., 2010; Nag et al., 2010; Wu et al. 2012; Wu et al., 2014; Karunarathne et al., 2015; Leal et al., 2019). Based on these studies, positive NBEs typically occur in the altitude range of 7–16 km while negative NBEs typically occur at altitudes of 14–20 km. Bandara et al. (2019) reported that negative NBEs sometimes occur at much lower altitudes, 4–8 km.

Positive NBEs were originally reported to occur as single isolated events (e.g., Le Vine, 1980; Willett et al., 1989; Smith et al., 1999). However, more recent studies suggest that NBEs often are associated with other lightning processes. In particular, positive NBEs initiate, or occur as the first event in, some intracloud (IC) lightning flashes (e.g., Rison et al., 1999; Nag et al., 2010; Wu et al., 2014; Karunarathne et al.,

---

2015; Rison et al., 2016). Wu et al. (2014) found that 103 out of 638 positive NBEs initiated IC flashes. Karunarathne et al. (2015) found that only 84 of 226 positive NBEs were isolated in time and space from other lightning events. Low altitude (4–8 km) negative NBEs initiate some negative cloud-to-ground (CG) flashes (Bandara et al., 2019).

The finding that NBEs are powerful HF and VHF intracloud lightning events has been confirmed by satellite measurements (e.g., Jacobson, 2003) and by ground-based measurements (Rison et al., 1999; Thomas et al., 2001; Rison et al., 2016; Bandara et al., 2019). Using a VHF lightning mapping array (LMA) operating at 60–66 MHz, Thomas et al. (2001) observed a positive NBE with a peak VHF power > 300 kW, and Rison et al. (2016) found three positive NBEs with peak powers of 93, 158, and 274 kW. For comparison, Thomas et al. (2001) showed that non-NBE pulses in typical IC flashes had LMA source powers of 1–10,000 W, while non-NBE pulses in CG flashes typically had LMA source powers < 500 W. Using a VHF sensor operating at 186–192 MHz, Bandara et al. (2019) found high-altitude negative NBEs had source powers of 260–7400 W while low-altitude negative NBEs that initiated negative CG flashes had source powers of 1–1300 W. Note that Le Vine (1980) did not characterize the HF or VHF waveforms of the NBEs he studied.

In this study we focus on measurements of 201 positive NBEs collected in 2016 in northern Mississippi, USA. Since VHF waveforms of NBEs have not received much attention, we especially focus on these waveforms and the corresponding VHF power. We compare the NBE properties obtained from E-change data (including 10–90% rise time, duration, and zero-crossing time) to the corresponding properties obtained from VHF data. Using the E-change waveforms, we classify our NBEs into Types A, B, C, and D (Karunarathne et al., 2015) and then examine and compare the NBE characteristics, including VHF source power, of each type. Furthermore, using data from the sensor array, we locate each NBE in space and time; these locations allow us to divide the positive NBEs into three spatiotemporal groups relative to other lightning activity. We then compare VHF source power and other characteristics across these spatiotemporal categories to determine whether NBEs in these groups are similar or different.

2. Instruments

In June through September 2016, we deployed a lightning sensor array in and around Oxford, Mississippi. A detailed description of the lightning sensing array and the accuracy of lightning event locations, along with a discussion of the initiation characteristics of two IC and two CG flashes, can be found in Marshall et al. (2019). Here we briefly summarize the instrumentation. The array was composed of seven lightning sensing stations (see black stars in Fig. 1a); each station was identified by a two or three-character code. The five inner sites (EE, FS, IH, JM, and TM) of the array spanned an area of 20 km × 20 km, while the other two sites (SS and NDS) expanded the array to an area of roughly 60 km × 30 km. Each station was equipped with four sensors: a flat plate E-change sensor ("fast antenna" or "FA") with an electronic decay time constant of 10 ms, a flat plate E-change sensor ("slow antenna") with a 1 s decay time constant, a flat plate sensor for the time derivative of the electric field ("dE/dt"), and a vertically oriented, omnidirectional disc-cone antenna for VHF measurements ("Log-RF"). The sensors at each site were triggered whenever a floating threshold was exceeded in the site's FA data. Each data record for all sensors was 400 ms long with 250 ms of pre-trigger and 150 ms of post-trigger and was time-stamped using GPS timing (1 sigma average of less than 2 ns). Lightning data of each sensor were digitized at 10 MegaSamples/s (MS/s) with a 12-bit digitizer. The fast and slow antennas had bandwidths of 16 Hz – 2.6 MHz and 0.16 Hz – 2.6 MHz respectively; for these two sensors, successive pairs of data were averaged before being recorded (making an effective sampling rate of 5 MS/s). The dE/dt sensor had a bandwidth of ~0–2.5 MHz. The Log-RF sensor was a logarithmic power sensor with a VHF bandwidth of 186–192 MHz.

The present study is based on NBE data that were recorded during July and August 2016 using the seven-station lightning detection array. Short-duration lightning pulses, including NBEs, were located in time and space using a time-of-arrival technique called Position By Fast Antenna or PBFA (Karunarathne et al., 2013), which uses FA data from at least 5 sensor sites. Using the technique described in Bandara et al. (2019), we also located lightning events by first integrating the dE/dt data with respect to time (to get another measure of *E*-change) and then feeding the integrated data into the PBFA algorithm. In this study, NBEs and other lightning pulses were located using the $\int dE/dt$ or FA data, depending on availability of triggered data and their signal-to-noise ratio.

3. Method of Identifying NBEs

Previous studies (e.g., Smith et al., 2002; Hamlin et al., 2007; Wu et al., 2011; Wu et al., 2014; Karunarathne et al., 2015; Leal et al., 2019) have identified positive NBEs with various automated search routines using E-change data. However, since NBEs are known to be strong VHF sources, in this study we used both E-change and Log-RF data to identify positive NBEs.

The triggered Log-RF data obtained at the EE station were used to find possible candidates for positive NBEs. In each record, we programmatically searched for Log-RF pulses having peak amplitude greater than five times the threshold level. The threshold level used in this procedure was an arbitrary value and was adjusted to find only large Log-RF pulses in which the initial polarity of the corresponding FA waveform was positive in keeping with a positive NBE. Furthermore, we required that at least five different sensor sites triggered on each candidate event so that we could locate it using either PBFA or integrated dE/dt. We also required that each candidate event have horizontal location errors Δx and Δy < 2 km and chi-squared goodness-of-fit values < 5.

Finally, we carefully examined the coincident FA waveform associated with each possible NBE to make sure that it was consistent with previously reported positive NBE waveforms (e.g., Le Vine, 1980; Willett et al., 1989; Medelius et al., 1991; Smith et al., 1999; Smith et al., 2004; Ahmad et al., 2010; Nag et al., 2010; Karunarathne et al., 2015; Leal et al., 2019). A large number of Log-RF records were processed using the automated algorithm described above, and the consistency check procedure yielded a set of 201 positive NBEs.

Fig. 1a shows the horizontal plan view of the 201 positive NBEs. As described in the next section, 188 NBEs are color-coded by waveform Types A, B, C, and D (Karunarathne et al., 2015). Fig. 1b shows an altitude histogram of the 188 NBEs of Types A to D, including the average altitude and standard deviation for each type. The horizontal distance (D) from the EE site of the positive NBEs ranged from 6 to 80 km with altitudes of the NBEs varying from 5.0 to 15.5 km. Fig. 1b shows that Type B NBEs occur on average at substantially higher altitudes than the other types of NBEs, while the three Type A NBEs are significantly lower in altitude than most other NBEs. Fig. 1c and d show, respectively, the horizontal (ΔD) and vertical (Δz) location errors of the 201 positive NBEs with ΔD < 2 km and Δz < 1.5 km.

4. Results

4.1. Categorization of NBEs into Types A, B, C, and D

As described above the basic fast antenna (FA) waveform of a positive NBE has a bipolar shape with a leading, "main" positive peak followed by a smaller, negative, "overshoot" peak (in the physics convention of electric field, used herein). Karunarathne et al. (2015) divided 226 positive NBEs observed on a single day in Florida into four categories (Types A to D) according to their characteristic E-change waveforms; examples of these types from the data used herein are shown in Fig. 2. Type A NBEs have the classic bipolar waveform. Type B
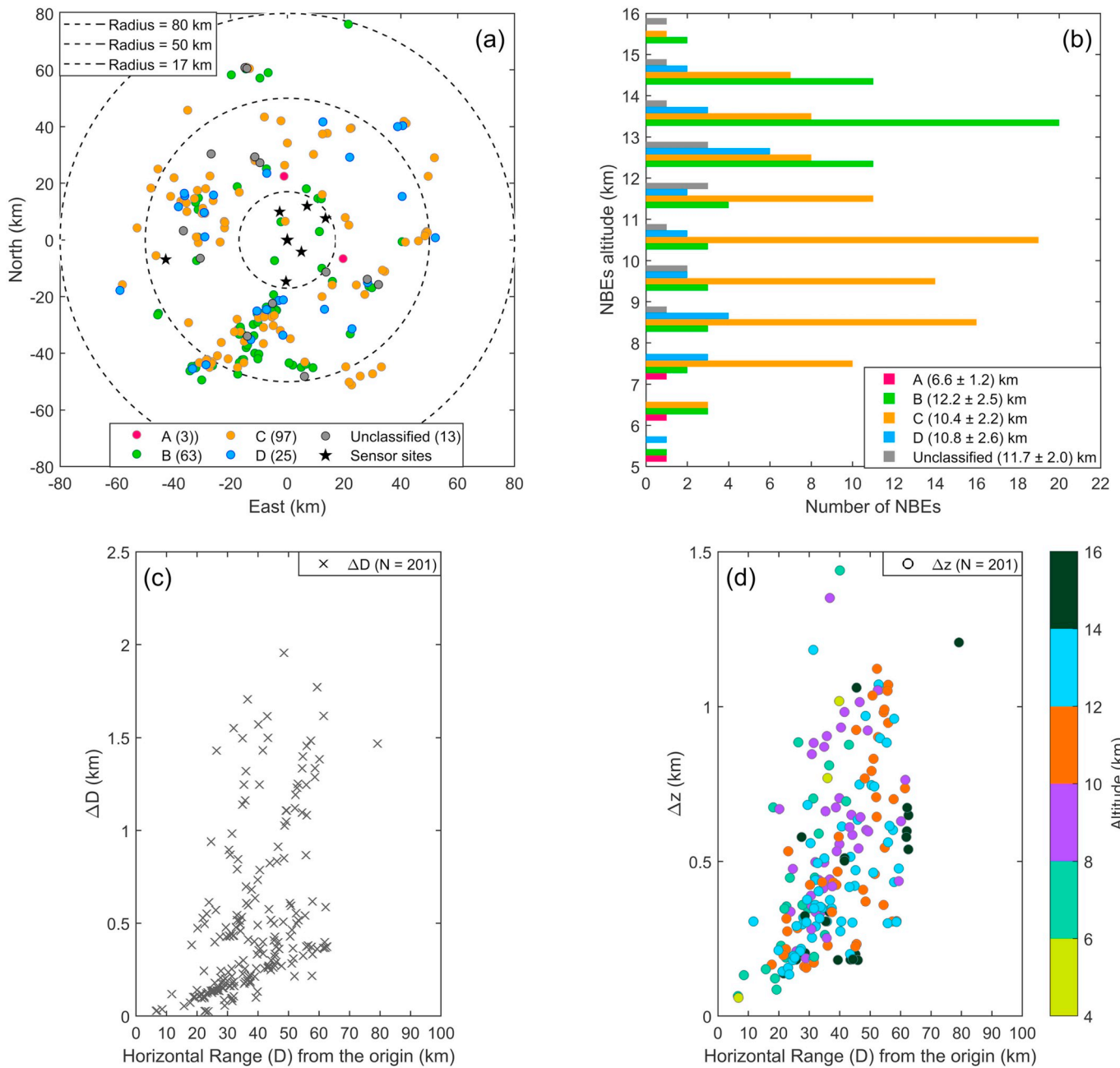
Fig. 1. (a) Plan view of seven sensor sites (marked with stars) along with locations of 201 positive NBEs. The central sensor site, EE, is located at the origin of the coordinate system; three range rings are also shown. Types A to D NBEs are marked with red, green, orange, and light blue dots, respectively, with 13 unclassified NBEs marked in gray. (b) Histogram of NBE altitudes colored by Type. Legend shows average NBE altitudes and standard deviations by Type. (c) Horizontal distance error (ΔD) marked as " × " for 201 NBEs. (d) Altitude error (Δz) for 201 NBEs are marked with dots color-coded according to NBE altitude (see color bar). (For interpretation of the references to color in this figure legend, the reader is referred to the web version of this article.)

NBEs have one or more additional positive peaks just after the negative overshoot, which gives a noticeable oscillatory shape at the end of the classic bipolar waveform (e.g., Medelius et al., 1991; Hamlin et al., 2007; Nag and Rakov, 2010). Type C NBEs have an additional pulse or pulses just after the main positive peak or between the main peak and the negative overshoot in the bipolar waveform (e.g., Medelius et al., 1991; Ahmad et al., 2010). Type D NBEs have a significant extra peak or peaks just prior to the main positive peak in the bipolar waveform. Additionally, Karunarathne et al. (2015) noted that some NBEs can have two types simultaneously, e.g., Type D + B. Recently, Leal et al. (2019) categorized 1022 positive NBE E-change waveforms into eleven categories with Types 1–4 being the same as Types A to D, respectively, and Type 5 and Type 6 being identical to Type C + B and Type D + B.

The five new types (#7–11) identified by Leal et al. (2019) were relatively rare in their dataset, together totaling only 58 of the 1022 positive NBEs.

We have categorized 188 of the 201 positive NBEs as Types A to D; as in Karunarathne et al. (2015) NBEs of Type C + B and Type D + B were categorized as Type C and Type D, respectively. The remaining 13 positive NBEs could not be readily identified as any of the Types A-D and are referred to as "unclassified" herein. (Most of these 13 NBEs would fit into types 7 to 11 in the more recent study of Leal et al. (2019).) We call this classification "Method 1." Table 1 shows the distribution of the 188 positive NBEs into Types A to D according to Method 1. For comparison, Table 1 also includes the Types A to D distribution of 226 positive NBEs observed by Karunarathne et al.
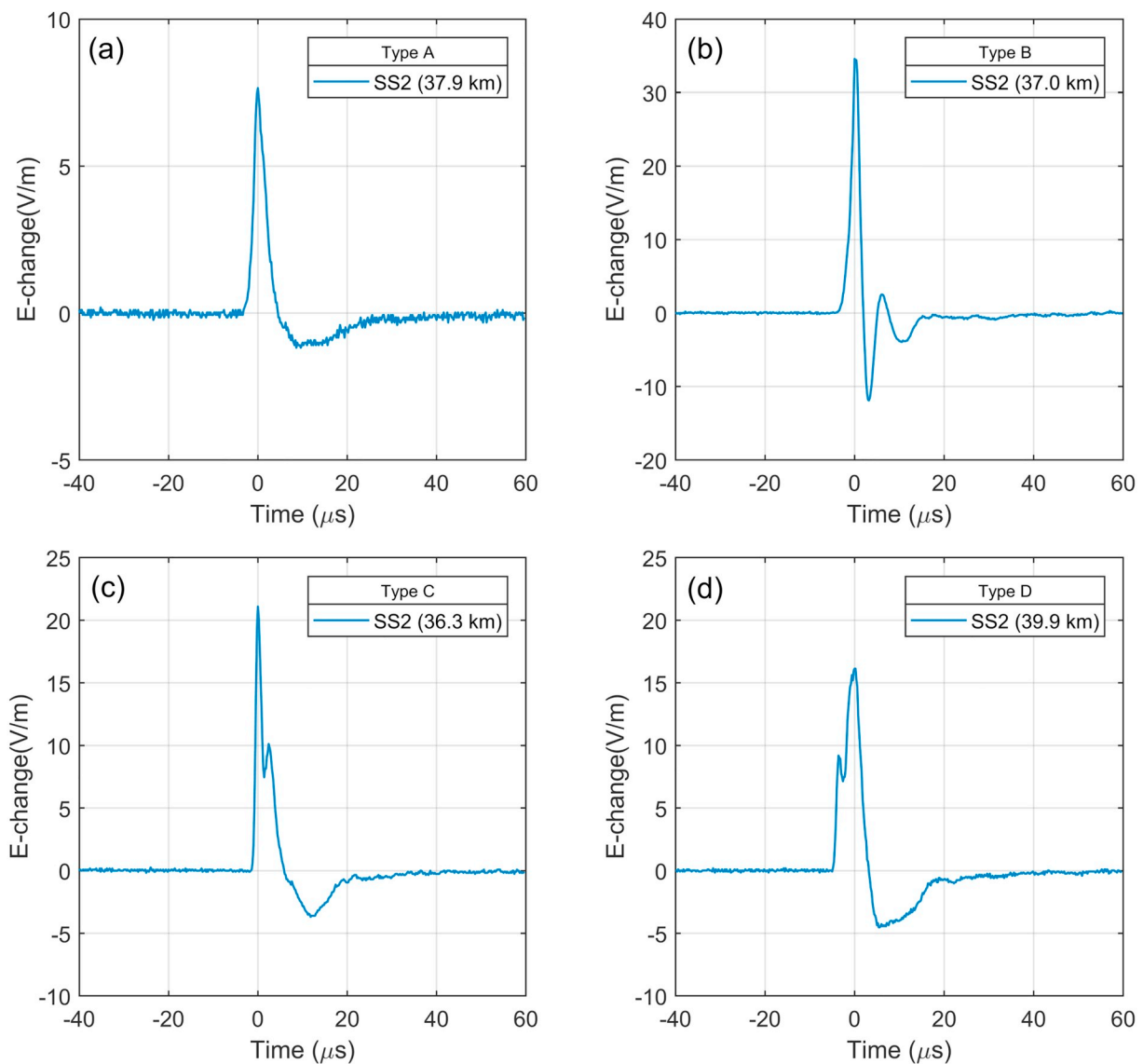
Fig. 2. Examples of Types A–D NBEs; data collected at the SS sensor site. In each plot, the number in parenthesis indicates the horizontal distance of the NBE to the SS.

Table 1
Classification of NBEs using Method 1.

Method 1	Number of NBEs		
	Current study (188 NBEs)	Karunarathne et al. (2015) (226 NBEs)	Leal et al. (2019) (964 NBEs)
Type A	3 (2%)	2 (1%)	263 (27%)
Type B	63 (34%)	151 (67%)	443 (46%)
Type C	97 (52%)	30 (13%)	164 (17%)
Type D	25 (13%)	43 (19%)	94 (10%)
Unclassified	13 (6.5% of 201)		

(2015) and of 964 NBEs of Types 1–6 observed by Leal et al. (2019). For our 188 NBEs, the distribution by percentage of NBE Types from greatest to least was: C, B, D, A, while the distribution for the Karunarathne et al. (2015) was B, C, D, A and for Leal et al. (2019) was B, A, C, D. In our set of NBEs and in the Karunarathne et al. (2015) set, simple bipolar Type A NBEs were rare (< 2%); in contrast, this type is the most common waveform shown in several NBE studies (e.g., Smith et al., 1999, 2004; Nag et al., 2010) and is the second largest group

(27%) of 964 NBEs in Leal et al. (2019). Karunarathne et al. (2015) speculated that Type A NBEs were rare in their NBE set for one or both of the following reasons: (i) Type A NBEs have relatively small amplitudes and therefore might be missed by their search algorithm that was biased to larger amplitude NBEs, or (ii) the relatively short range to their NBEs (< 150 km with 90% of NBEs within 90 km) allowed better detection of smaller-scale features of Types B, C, and D. Since our 188 NBEs were all located within 80 km while the Leal et al. (2019) NBEs had a much wider range (< 500 km), the larger percentage of Type A NBEs in Leal et al. (2019) could be due to missing smaller-scale features of Types B, C, and D. It is also the case in this study, as in Karunarathne et al. (2015), that the few Type A NBEs had relatively small FA amplitudes compared to the other types (see Section 4.3).

4.2. Categorization of NBEs according to their spatiotemporal relationship with other lightning events

As discussed in Section 1, NBEs were originally considered to be isolated in time from other cloud discharges (e.g., Willett et al., 1989; Smith et al., 1999). However, more recent studies show that some of positive NBEs are related to or occur during lightning flashes (e.g.,
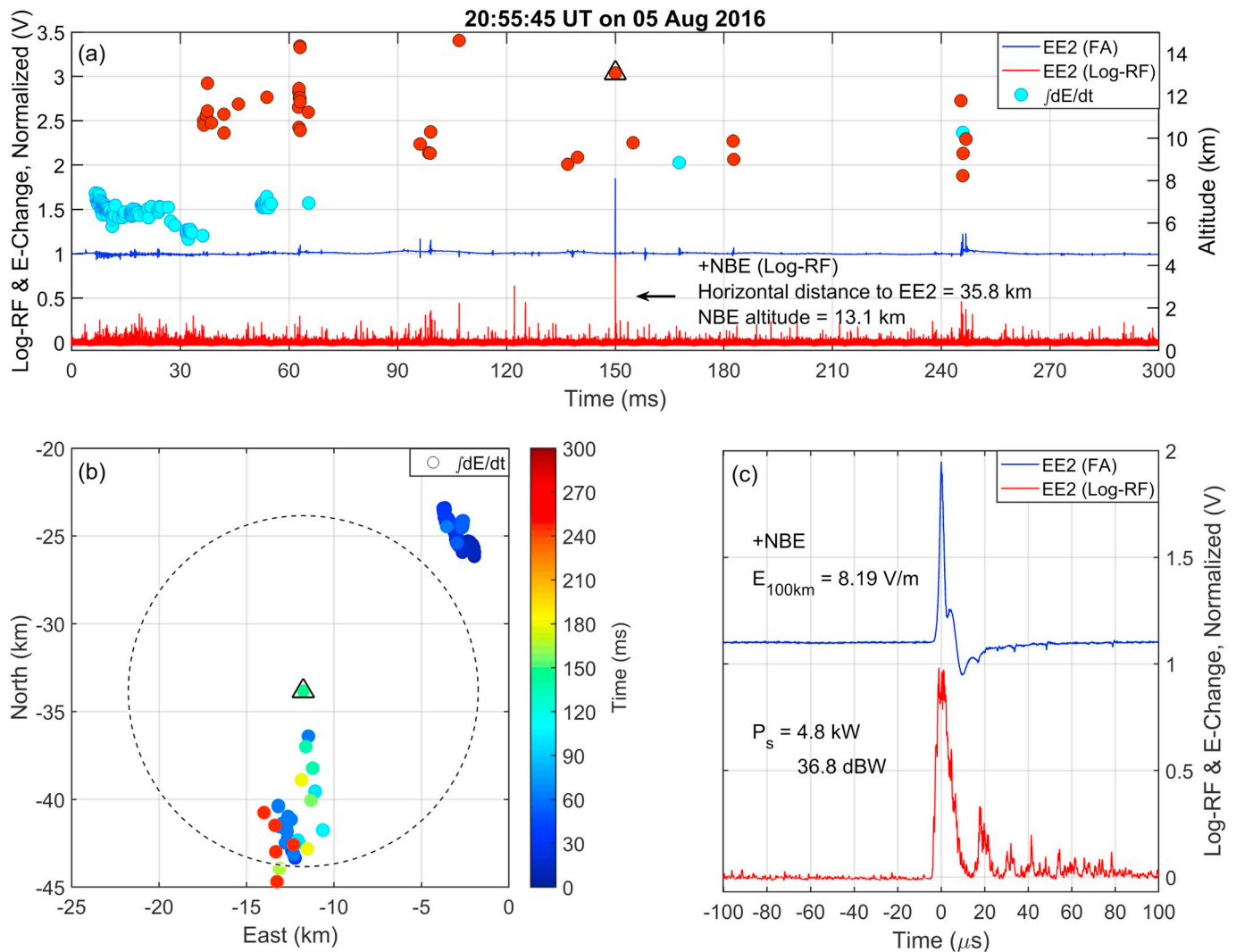
Fig. 3. Example of a "Not-Isolated" positive NBE (Type C plus B). (a) Overview showing 300 ms of FA data (blue) and Log-RF data (red) shown as normalized voltages. The light blue and red-brown dots denote the altitudes (right axis) of the FA pulses determined by $\int dE/dt$ with red-brown dots for pulses within 10 km horizontally from the NBE and light blue for pulses > 10 km from the NBE. (b) Plan position plot of the lightning events shown in (a). The NBE is in the center and marked with a small black triangle, and the circle shows 10 km range from the NBE. The other located pulses are color-coded for their occurrence time (see vertical color bar at right). (c) Expanded view (200 µs) of the NBE with E-change (FA) amplitude of 8.19 V/m (range normalized to 100 km) and Log-RF (VHF) power of 4.8 kW. (For interpretation of the references to color in this figure legend, the reader is referred to the web version of this article.)

Rison et al., 1999; Nag et al., 2010; Wu et al., 2014; Karunarathne et al., 2015; Rison et al., 2016). Karunarathne et al. (2015) investigated the isolation in space and time of their 226 positive NBEs from other lightning events: an NBE was classified as "isolated in space" if no other lightning event occurred within 10 km horizontally of the NBE and classified as "isolated in time" if no other lightning activity occurred within ± 660 ms of the NBE. (The time of 660 ms was used because it is a typical duration of IC flashes.) Using these same isolation parameters, we developed a spatiotemporal method ("Method 2") of categorizing our positive NBEs. This categorization used lightning event locations given by PBFA using FA and/or $\int dE/dt$ data. Method 2 divided the NBEs into three groups called "Isolated," "INBE," and "Not-Isolated." An NBE was in the Isolated group if it did *not* have any other detectable lightning events (pulses) within 10 km horizontally or within ± 660 ms in time. The INBE group included all NBEs that initiated IC flashes (e.g., Rison et al., 1999; Wu et al., 2014), in the sense that they were the first event in the flash. The remaining NBEs that were neither isolated nor first in an IC flash were in the 'Not-Isolated' group. Hence, it should be noted that our "Not Isolated" group does not include INBEs.

We applied Method 2 to the 188 positive NBEs classified as Types A

to D by Method 1. Of the 188 NBEs, we were unable to use Method 2 on 42 NBEs because we were unable to fully test their spatial relation of events within 10 km; this occurred when there were not enough triggered sensors to provide locations of very small lightning pulses. Thus the number of NBEs with spatiotemporal categorization was 146.

4.2.1. "Not-Isolated" NBEs

There were 51 NBEs in the Not-Isolated category or 34.9% of the 146 NBEs considered with Method 2. Fig. 3a shows an example of a Not-Isolated NBE that occurred within 10 km of and during an IC lightning flash. The NBE occurred at 13.1 km altitude and was located 35.8 km from the EE site. In Fig. 3a the NBE is marked with a triangle and located at time 150 ms (of the 300 ms displayed). In Fig. 3a the lightning pulses in the FA data marked with light blue dots occurred more than 10 km from the NBE while pulses marked with dark red dots occurred within 10 km of the NBE. Fig. 3b shows the horizontal locations of all the events in Fig. 3a, with the events color-coded by time. The NBE's position is indicated by the triangle, and the dotted circle shows the 10 km radius from the NBE. Therefore, all lightning events indicated by dark red dots in Fig. 3a are within the circle in Fig. 3b.
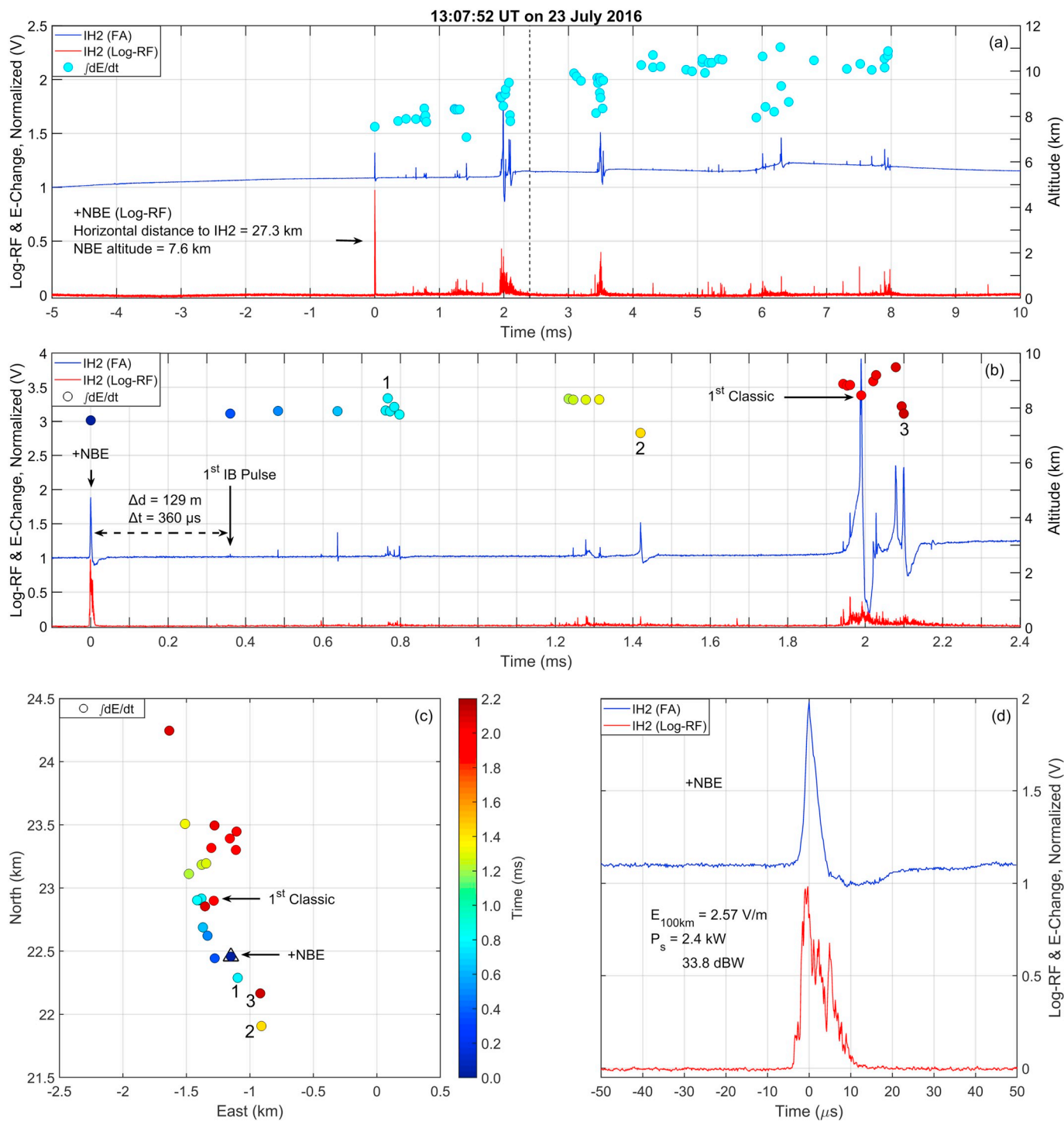
Fig. 4. Example of a positive NBE (Type A) that occurred as the initial event (INBE) of an IC flash. The FA data (blue) and the Log-RF data (red) are shown as normalized voltages. (a) 15 ms of the IC flash including 5 ms of pre-INBE data and 10 ms of post-INBE data. The altitudes of the FA pulses (light blue dots) are given on the right axis and were determined using ∫ dE/dt. (b) Expanded view (2.5 ms) of INBE and first IB pulses including the first two classic IB pulses. Located events are color-coded by time using color bar in part (c). (c) Plan view (3 km × 3 km) of locations shown in (b). (d) Expanded view (200 μs) of the NBE with FA amplitude of 2.57 V/m (range normalized to 100 km) and VHF power of 2.4 kW. (For interpretation of the references to color in this figure legend, the reader is referred to the web version of this article.)

Based on Fig. 3a and b, there were two IC flashes during the 300 ms. The first IC flash occurred about 12 km northeast of the NBE location; most of this flash's development occurred from 150 to 110 ms before the NBE in the altitude range of roughly 6–8 km. About 110 ms before the NBE, the second IC flash began almost 10 km due south of the NBE location, at an altitude of about 11 km, and it then propagated northward, mainly at altitudes between 8 and 11 km with a few pulses located above 14 km. The last two pulses before the NBE were 3–4 km south of it and 4 km below it. It seems possible (and even likely) that the approaching negative polarity breakdown of the southern IC flash triggered (or helped trigger) the positive NBE. Thus, at least some positive NBEs in our Not-Isolated group may have occurred because of nearby lightning events.

Fig. 3c shows the waveforms of FA and Log-RF data associated with

Table 2

Comparison of Method 1 classification with Method 2.

Method 2	Method 1			
	A (3)	B (63)	C (97)	D (25)
INBE (74)	3	14	49	8
Not-Isolated (51)	0	26	20	5
Isolated (21)	0	8	11	2
Unknown (42)	0	15	17	10

NBE on a 200 μs scale. The NBE had a range-normalized FA amplitude (E_{100km}) of 8.19 V/m and a VHF power of 4.8 kW (36.8 dBW). This NBE was Type (C + B). As is typical of our VHF logarithmic power measurements, the main NBE peak was quite 'noisy' compared to the smooth bipolar FA pulse. This NBE was somewhat unusual because of the multiple LogRF peaks occurring for almost 80 μs after the main peak; note that the bipolar FA NBE waveform duration was < 30 μs. As is typical, the first peak in the LogRF data (at 0 μs) was coincident with the main positive peak of the bipolar NBE (in the FA data), as discussed later. The second peak in the LogRF data at ~18 μs was coincident with a downward peak in the FA data (associated with the Type B designation); note that this second LogRF peak was much wider than the coincident downward FA peak. After this pair of peaks, there are multiple LogRF peaks for another 60 μs and some small FA peaks. We do not have explanation of the multiple LogRF peaks that follow the second

peak, but we note that these peaks last for a much longer time than the NBE "bouncing wave" oscillations reported by Nag and Rakov (2010, see their Fig. 1), which lasted only 5 μs. (Positive NBEs with multiple LogRF peaks, like those seen in Fig. 3c, are the subject of a separate study.)

4.2.2. "INBEs"

Wu et al. (2014) defined an INBE as a positive NBE that initiated an upward propagating IC flash within 10 ms of the NBE. Wu et al. (2014) determined that most of their INBEs occurred below 10 km altitude, while most of their other positive NBEs occurred above 10 km altitude. The upward propagation of the IC flash consisted of a series of "preliminary breakdown pulses," called initial breakdown pulses or IB pulses herein. We divide IB pulses into two types: classic and narrow (Nag et al., 2009). Classic IB pulses are bipolar with a duration ≥ 10 μs and an amplitude > 25% of the largest IB pulse amplitude in the flash (e.g., Kolmasova et al., 2019). Narrow IB pulses have durations < 10 μs and have amplitudes smaller than classic IB pulses (usually much smaller).

We found 74 NBEs that satisfied the INBE characteristics (50.7% of 146 positive NBEs). Fig. 4a shows an example of the first 10 ms of one of the IC flashes that started with an INBE. This Type A NBE occurred at an altitude of 7.6 km. The first IB pulse in the IC flash occurred 360 μs after the NBE, and subsequent IB pulses were sequentially higher in altitude. Thus, the NBE fits the INBE definition of Wu et al. (2014). As shown in Fig. 4d, the INBE had a range-normalized FA amplitude
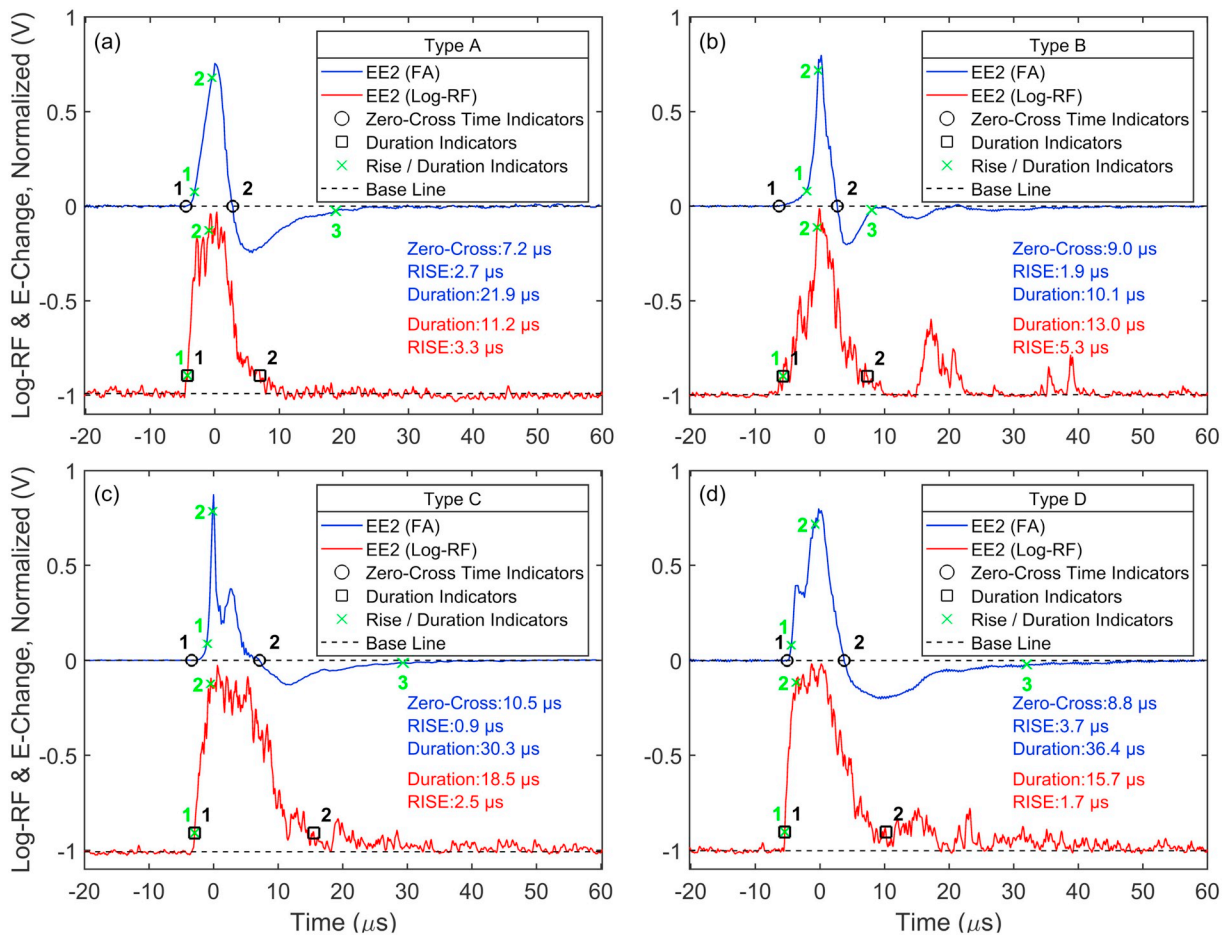

Fig. 5. Examples showing how rise time (10% to 90% of maximum amplitude), duration, and zero cross time are determined for Types A-D waveforms for FA data, and how rise time and duration are determined for the Log-RF data. The beginning and ending times for the zero-cross time of the FA waveforms and of the durations of the Log-RF waveforms are indicated with black circles, while the beginning and ending times for the rise time are indicated with the green "×" numbered "1" and "2" for both waveforms. The FA waveform durations are indicated by the green "×" numbered "1" and "3." (For interpretation of the references to color in this figure legend, the reader is referred to the web version of this article.)

Table 3
Comparison of FA waveform properties of positive NBEs.

|	Type (#)	Peak amplitude (V/m)	Rise time (µs)	FWHM (µs)	Zero cross (µs)	Pulse duration (µs)
Current study Mississippi (USA)	A (3)	2.0 ± 0.6	2.0 ± 0.2	3.2 ± 0.1	8.7 ± 2.0	30.1 ± 5.4
(Number = 188)	B (63)	8.6 ± 5.1	2.3 ± 0.9	2.3 ± 0.8	8.4 ± 3.9	32.4 ± 10.7
	C (97)	7.6 ± 3.3	1.9 ± 0.8	3.5 ± 1.9	9.6 ± 3.3	32.8 ± 10.5
	D (25)	7.4 ± 2.6	3.9 ± 1.5	4.6 ± 2.0	9.3 ± 2.6	33.5 ± 10.6
Current study (for all 201 NBEs)	Avg (201)	8.0 ± 4.0	2.4 ± 1.5	3.3 ± 2.0	9.7 ± 5.5	33.4 ± 11.9
Karunarathne et al. (2015) Florida	A (2)	12.2 ± 1.1	2.0 ± 0.0	3.1 ± 1.3	7.3 ± 1.0	–
(USA) (Number = 226)	B (151)	12.4 ± 6.8	2.4 ± 1.3	2.0 ± 0.7	9.0 ± 4.2	–
	C (30)	8.4 ± 3.9	1.5 ± 1.1	4.6 ± 2.6	12.7 ± 5.6	–
	D (43)	8.4 ± 4.1	4.3 ± 3.1	4.0 ± 1.6	11.1 ± 5.2	–
	Avg (226)	11.0 ± 6.2	2.6 ± 2.0	2.8 ± 1.8	9.9 ± 4.8	–

*Avg - average value for full set of NBEs.
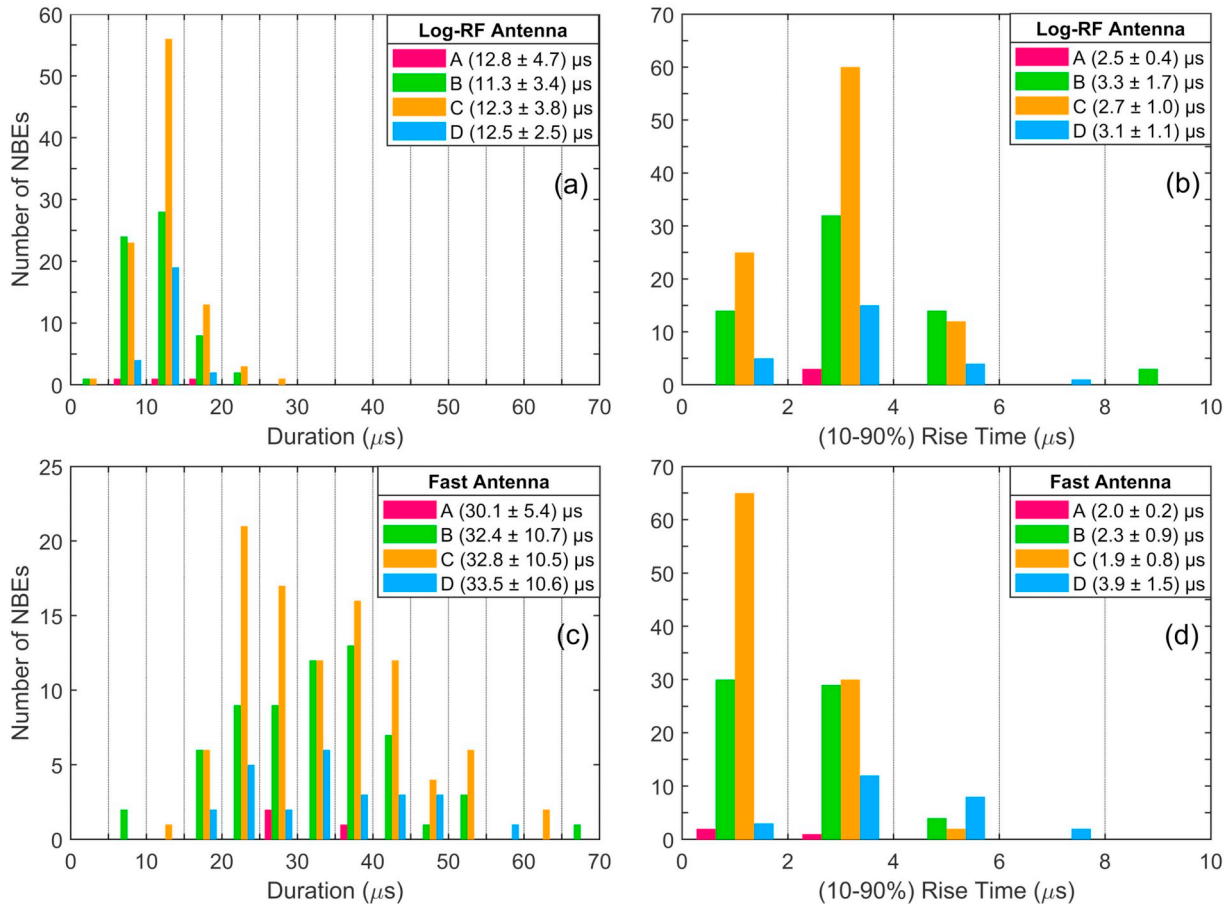
Fig. 6. Comparison of duration and rise time of Type A-D waveforms using Log-RF (Top) and FA (bottom) data. The legend of each plot includes (parenthetically) the arithmetic mean ± standard deviation of relevant property. The grid lines in each figure show the bin edges.

(E_{100km}) of 2.57 V/m and a VHF power of 2.4 kW (33.8 dBW).

The earliest 2.4 ms of development of this flash is shown in Fig. 4b and c. The time-altitude and horizontal positions of the pulses through the first 2.4 ms indicate the flash developed upward in two directions away from the INBE. One possible interpretation of this sequence of events is that the initial leader was branched, as has been observed in a few CG flashes (Stolzenburg et al., 2014). The first IB pulse, indicated in Fig. 4b, occurred 360 µs after the INBE. The first classic IB pulse occurred 1.98 ms after the INBE, was located about 1 km above and about 1 km north of the INBE, and had an FA amplitude about 10 times larger that the first IB pulse.

For our 74 INBEs the horizontal distance from the INBE to the first IB pulse ranged from 0.1 to 7.9 km with mean 1.0 km, while the time difference between the INBE and the first IB pulse varied from 0.2 to 6.7 ms with an average of 2.1 ms. About half (50.7%) of the 146

positive NBEs categorized using Method 2 were INBEs, which is much larger than the 16% INBEs found by Wu et al. (2014) in a group of 603 positive NBEs.

4.2.3. "Isolated" NBEs

As noted above, 51 of 146 positive NBEs were Not-Isolated and 74 NBEs were IBNEs, so the remaining 21 NBEs (14.3%) that could be classified by Method 2 were Isolated NBEs. The percentage of Isolated NBEs in this study is considerably smaller than the 37.2% of 226 positive NBEs found by Karunarathne et al. (2015). However, the small percentage of Isolated NBEs may be partly due to a bias caused by not being able to locate small pulses that occurred near in time to the NBE. Such NBEs are among the 42 "unknown" according to our Method 2. Thus, if all of the unknowns were in fact Isolated, then the percentage Isolated NBEs in this study, 33.5% (of 188), would be close that found
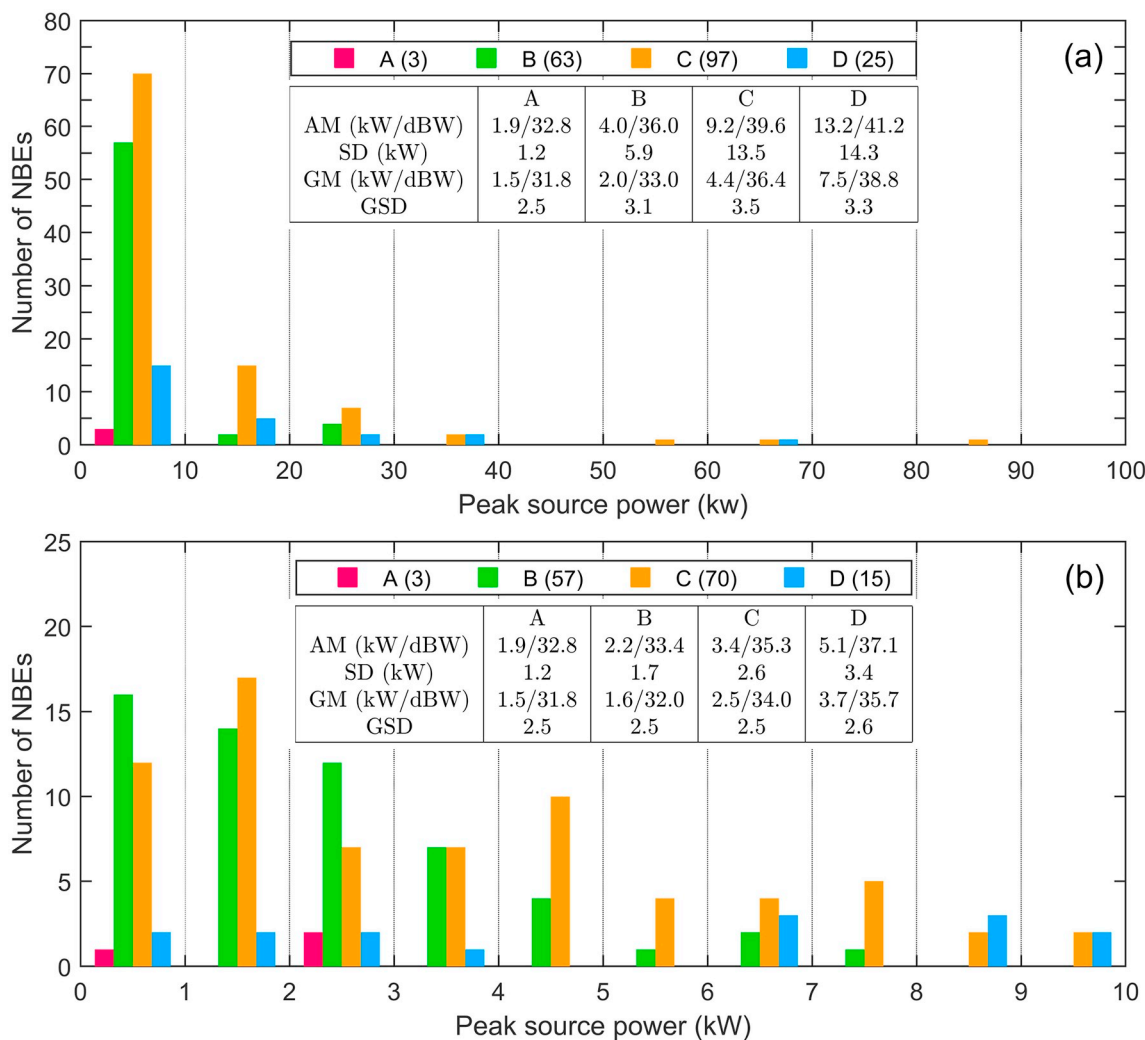
Fig. 7. (a) Distribution of peak radiated power for the Types A-D of NBEs. (b) An expanded view of 0–10 kW. The legend of each graph includes the number of NBEs (in parentheses) in the table, the arithmetic mean (AM), the geometric mean (GM), the standard deviation (SD) and the geometric standard deviation (GSD) for powers related to each type.

by Karunarathne et al. (2015).

Table 2 compares the positive NBEs categorized according to Method 1 (Types A to D) with the categorization of Method 2 (INBE, Not-Isolated, and Isolated). The INBE group was dominated by Type C NBEs (66%); in addition, all three Type A NBEs were INBEs and about half of the Type D NBEs were INBEs. Both the Not-Isolated and Isolated groups were primarily populated by Types B and C NBEs.

4.3. Positive NBE waveform properties

In this section we investigate the properties of both the E-change (FA) data and the VHF (Log-RF) data of the 201 NBEs. Positive NBE waveform properties based on FA data, i.e., the bipolar waveform, have been reported in many prior studies (e.g. Willett et al., 1989; Smith et al., 1999; Nag et al., 2010; Ahmad et al., 2010; Karunarathne et al., 2015). We know of no prior studies of positive NBE waveform properties based on VHF data.

4.3.1. Electric field change waveforms of positive NBEs

For FA data we determined five properties: range normalized peak amplitude, rise time, FWHM (full width at half maximum), zero-cross time, and duration. The first four properties are associated with the leading positive peak of the positive NBE while the duration is for the full bipolar waveform. With R being the slant range from the NBE to the

FA sensor, the measured peak amplitude was range-normalized to 100 km using a $1/R$ normalization; we denote this amplitude as E_{100km}. The rise time was determined as the time from 10% to 90% of peak amplitude, as marked with green x's numbered '1' and '2' in Fig. 5. FWHM was the width in time of the positive peak at half its maximum amplitude. Zero-cross time spanned the time of the leading positive peak, as indicated by black circles '1' and '2' in Fig. 5. NBE pulse duration was the time from 10% peak amplitude of the positive peak of the bipolar NBE to 10% of peak amplitude of the negative overshoot peak of the NBE, as marked with green x's numbered '1' and '3' in Fig. 5.

The FA waveform properties of positive NBEs in Mississippi are shown in Table 3. All FA waveform properties were determined using FA sensors at a range > 20 km from the NBE so that the measurements would be primarily radiation field (i.e., with little or no electrostatic or induction contributions). The properties are given individually for Types A-D and overall for 201 NBEs. For comparison, Table 3 gives the corresponding values for 226 NBEs measured by Karunarathne et al. (2015) on one day in Florida.

From Table 3 we can see that all the time parameters for our NBEs were in reasonable agreement with those found in Karunarathne et al. (2015); this finding is generally true for comparisons to the other NBE studies mentioned above. However, the average peak amplitude, E_{100km}, for the 201 NBEs of this study (8.0 ± 4.0 V/m) was smaller than the E_{100km} averages of (11.0 ± 6.2), (15.0 ± 3.4), and
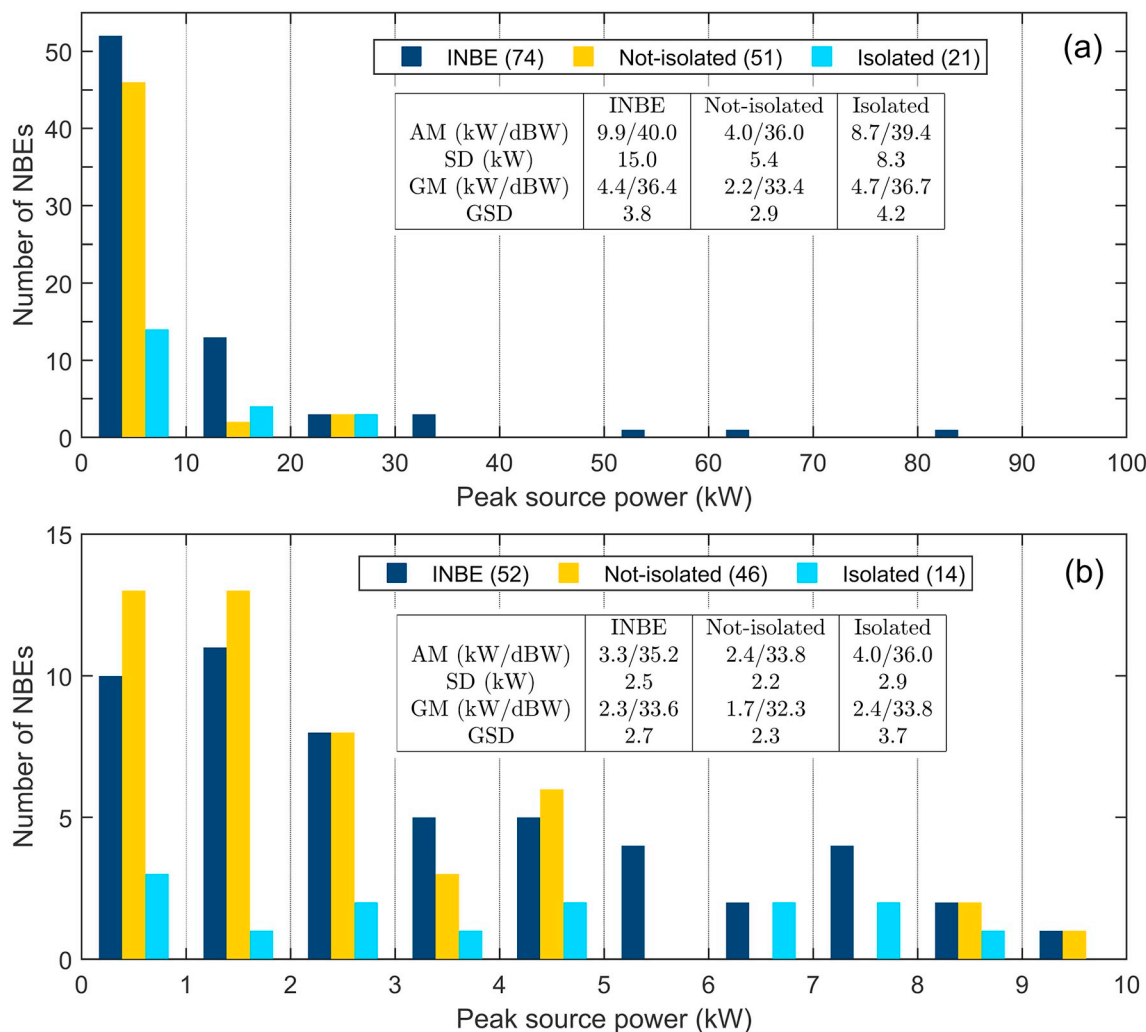
Fig. 8. Histograms of VHF powers of the three NBEs groups; INBE, Isolated, and Not-Isolated: (a) overall distribution, (b) expanded view of 0–10 kW. AM = arithmetic mean, SD = standard deviation of AM, GM = geometric mean, GSD = standard deviation of GM. The legend of each plot includes (parenthetically): in (a) number of NBEs in each group, in (b) number of NBEs that have peak power < 10 kW.

(22.7 ± 9.7) V/m reported by, respectively, Karunarathne et al. (2015), Nag et al. (2010), and Ahmad et al., (2010). On the other hand, our average peak amplitude value was in good agreement with the values of (8.0 ± 5.3) and (9.5 ± 3.6) V/m reported by Willett et al. (1989) and Smith et al. (1999). In descending order, the average peak amplitude for each NBE type was B, C, D, A.

4.3.2. VHF waveforms of positive NBEs

Since the Log-RF sensor measured VHF power, its NBE waveform was unipolar (Bandara et al., 2019). We compiled three Log-RF properties: rise time, duration, and peak power. The Log-RF rise time of each NBE was determined in the same way as for the FA NBE waveform, namely the time from 10% to 90% of peak amplitude (see green x's in Fig. 5). The Log-RF duration of each NBE was the time from 10% peak amplitude on the rising side of the NBE to 10% of peak amplitude on the falling side of the peak, as shown with black squares in Fig. 5. The Log-RF measurements for the 201 NBEs were obtained by averaging measurements from at least 4 sensor sites. Additionally, the data were downsampled to 1 MS/s.

The Log-RF duration of positive NBEs had an average and standard deviation of (12.1 ± 3.6) μs and a range of 3.7 to 28.1 μs. The mean rise time and standard deviation of Log-RF waveforms was (3.1 ± 1.5) μs with values varying from 1.1 to 8.9 μs.

There have been no previous studies of the VHF waveform

properties of positive NBEs with which to compare our findings. However, Bandara et al. (2019) studied three groups of negative NBEs with the same instruments used herein; the groups were (1) typical (high altitude) negative NBEs (labeled as NNBE(T)s), (2) low altitude negative NBEs (labeled as NNBE(L)s), and (3) low altitude hump-shaped negative NBEs (labeled as NNBE(H)s). The dividing line between low and high altitude negative NBEs was 8 km. We found that positive NBE Log-RF waveforms had average duration/standard deviation of (12.1 ± 3.6) μs, while the corresponding values in Bandara et al. (2019) for NNBE(H)s, NNBE(L)s and NNBE(T)s were somewhat smaller: (7.4 ± 2.8) μs, (10.5 ± 3.1) μs, and (8.3 ± 3.8) μs, respectively.

Fig. 6 compares the durations and rise times of Type A-D positive NBEs based on Log-RF data and on FA data. The VHF (Log-RF) data are associated with short charge motions (~1.6 m) while the E-change (FA) data are associated with longer charge motions (> 120 m) (e.g., Betz et al., 2008; Marshall et al., 2019). The average durations of the VHF (Log-RF) unipolar pulses were shorter (11–13 μs) than the bipolar E-change (FA) durations (30–35 μs). Fig. 6 also shows that for each positive NBE type the average rise time was similar for the Log-RF and FA waveforms.

Using the Friis transmission equation, the NBE source power was determined from the received NBE power (determined from the Log-RF peak voltage and the Log-RF sensor's power calibration) and the
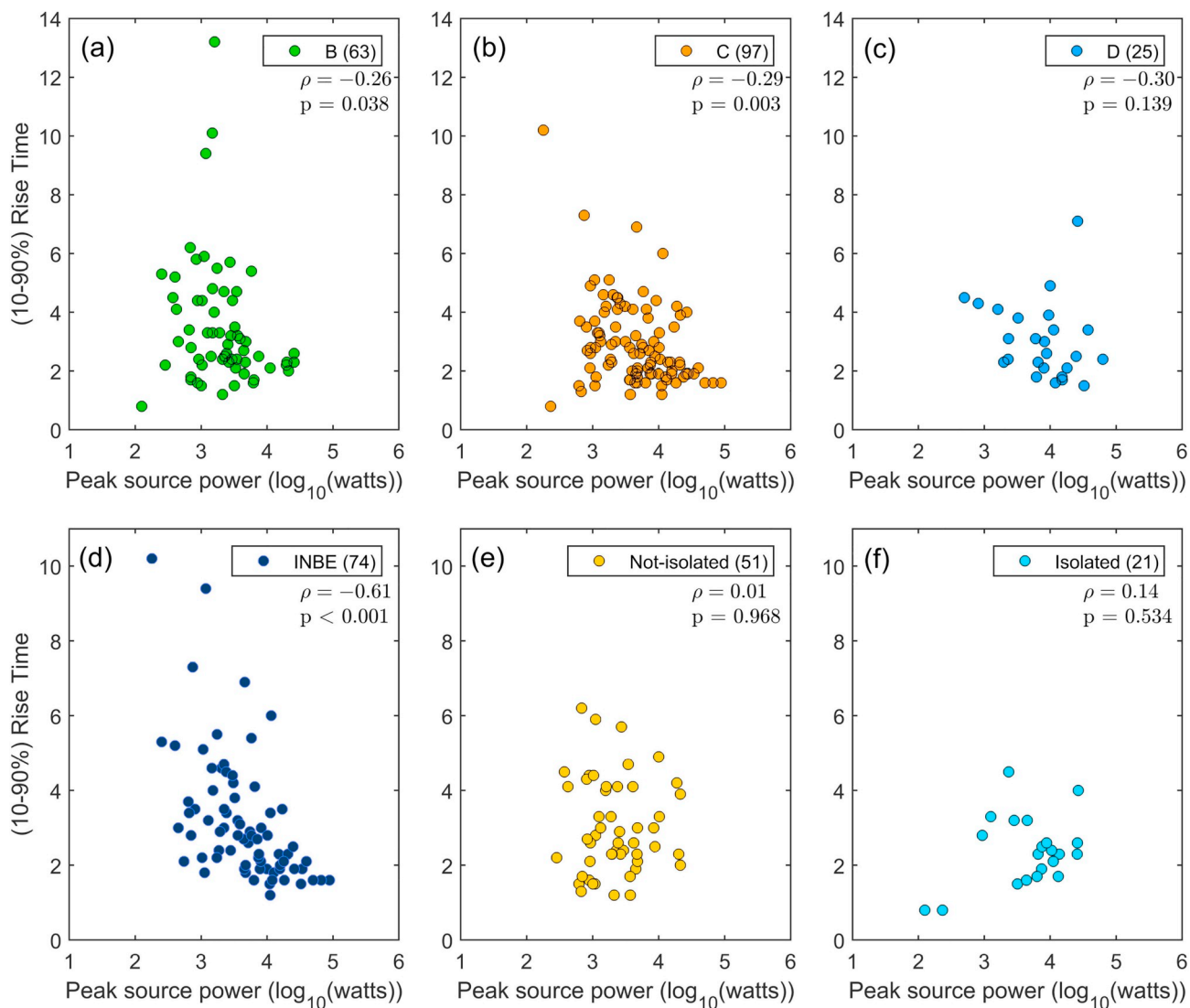
Fig. 9. Scatter plots of the peak radiated power versus the rise time of the Log-RF waveform. (a) – (c) Types B-D NBEs. (d)-(f) NBEs in INBE, Not-Isolated, and Isolated groups. The legend of each plot includes (in parentheses) the number of NBE found in each type or group. ρ = Spearman correlation coefficient. p = probability value.

distance of the NBE from the Log-RF sensor, as explained in Bandara et al. (2019). Fig. 7a shows a histogram of the radiated peak source powers for Types A-D of 188 NBEs (Method 1, Section 4.1). The largest NBE power was 88.4 kW, but 77% of the NBEs had powers < 10 kW (distribution shown in more detail in Fig. 7b). For each NBE type, the arithmetic mean (AM) with its standard deviation (SD) and geometric mean (GM) with its standard deviation (GSD) are listed in Fig. 7. Overall for the 188 positive NBEs, the VHF power had an AM of 7.9 kW (SD = 11.9 kW) and a range of 0.1–88.4 kW. The power of the three Type A NBEs was less than 3 kW, while the other three NBE Types ranged up to 30 kW with a few Type C and Type D NBEs having higher powers. In descending order the average power per NBE type was D, C, B, A (13.2, 9.2, 4.0, 1.9 kW), which is different from the order of the average peak electric field change, E_{100km}, of B, C, D, A (8.6, 7.5, 7.4, 2.9 V/m).

Since there have been no previous studies of the VHF peak powers of a large number of positive NBEs, we compare them to the powers of the three groups of negative NBEs (57 NBEs in all) studied by Bandara et al. (2019). For NNBE(H)s, NNBE(L)s, and NNBE(T)s, respectively, they found Log-RF power (ranges) of $(1-23)$W, $(9-1290)$W, and $(260-7420)$W, with arithmetic mean/standard deviation values of (9 ± 6)W, (234 ± 340)W and (1770 ± 2100)W. Fig. 7 shows that

almost all of the 188 positive NBEs studied herein had powers greater than those of the low altitude NNBE(H)s and NNBE(L)s and 56 (30%) of the positive NBEs herein had powers greater than the most powerful of the typical, high altitude, negative NBEs.

Using a format similar to that of Fig. 7, Fig. 8 shows the overall distribution of peak source power for the three NBE groups: INBE, Not-isolated, and Isolated (146 NBEs, categorized using Method 2 of Section 4.2). Once again 77% of the NBEs had VHF powers < 10 kW (see Fig. 8b). The powers of NBEs in the Not-isolated and Isolated groups were all < 30 kW while the INBE powers extended to 88.4 kW. However, 53% of INBEs had peak VHF power < 5 kW, so an INBE does not require a large power to initiate an intracloud flash. In descending order, the average power per NBE group was INBE, Isolated, Not-isolated. With a digital interferometer and a lightning mapping array, Rison et al. (2016) determined the VHF power (in the 60–66 MHz band) of 10 INBEs; their VHF powers extended to higher powers (up to 270 kW).

4.3.3. Comparison of Log-RF rise time and peak power of positive NBEs

In this section we investigate whether Log-RF rise time and peak power are correlated for positive NBEs. Fig. 9 shows scatter plots of the peak radiated power and rise time of the Log-RF waveforms for NBEs of
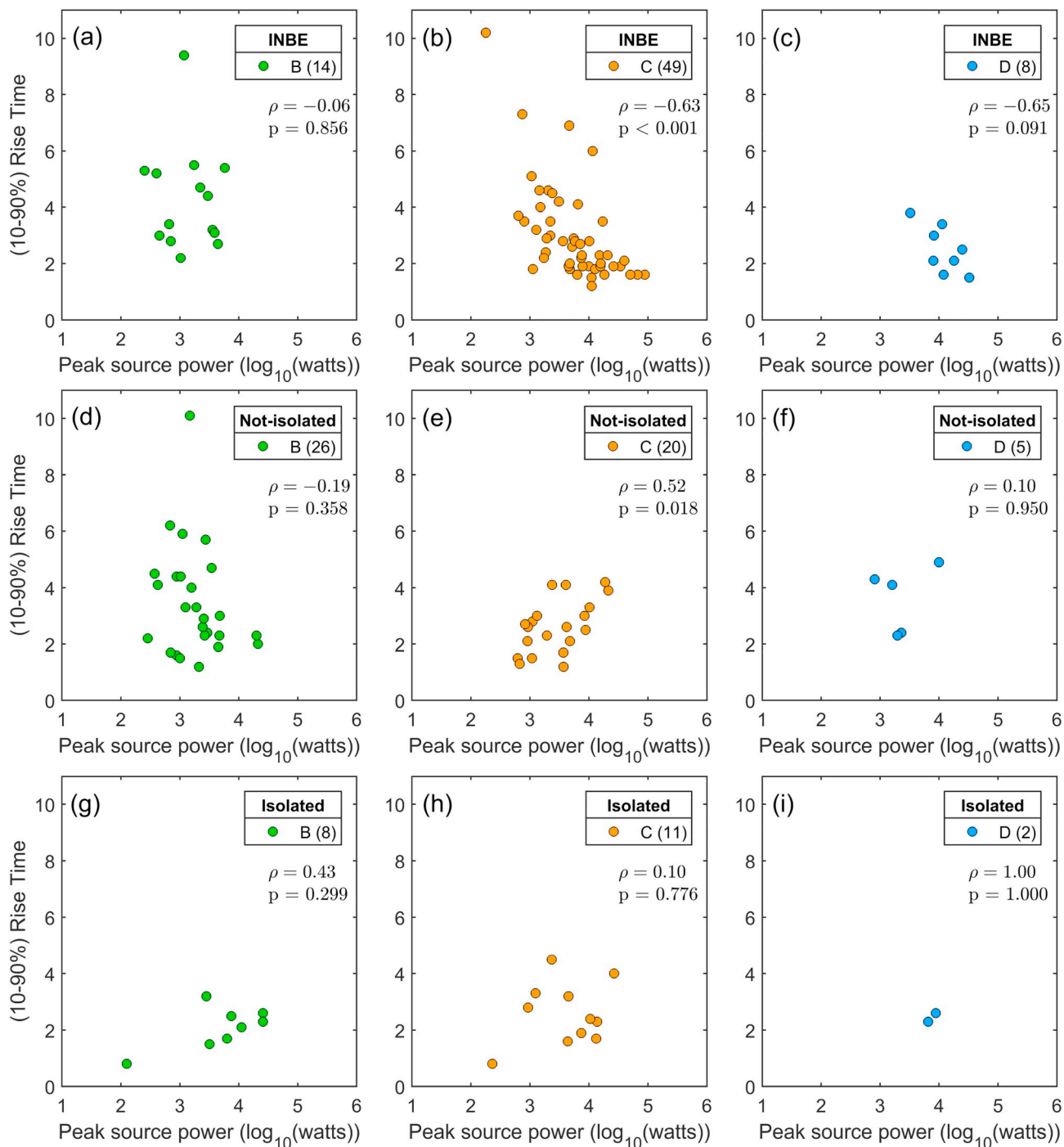
Fig. 10. Similar to Fig. 9, (a) – (c) Type B-D NBEs found in INBE group. (d)-(f) Type B-D NBEs found in Not-Isolated group. (g)-(i) Type B-D NBEs found in Isolated group. ρ = Spearman correlation coefficient. p = probability value.

Types B-D (Fig. 9a, b, and c), and for NBEs of Groups INBE, Not-Isolated, and Isolated (Fig. 9d, e, and f). There is a total of 185 Type B-D of NBEs and 143 NBEs in the INBE, Not-Isolated and Isolated groups. Type A NBEs were excluded from this comparison due to the small sample size.

The Spearman rank correlation coefficient, ρ, is a non-parametric statistical measurement, and it weighs (or ranks) the strength of the monotonic relationship between two data sets. The correlation coefficient ρ ranges between 1.0 (strong correlation) and 1.0 (strong anti-correlation) with zero indicating no correlation between the data sets. Additionally, the level of statistical significance is based on the probability value (p), which indicates the probability of random occurrence

of a correlation. A smaller *p* value indicates that a correlation between two data sets is not likely to be due to random occurrence; we required $p < .01$ for correlations.

In general Fig. 9 suggests that there is little or no correlation between NBE power and NBE rise time in the Log-RF waveforms. However, the Spearman correlation coefficients (ρ) of -0.29 and -0.61 and probability values (p) of 0.003 and 0.001 respectively for Type C NBEs and the INBE group indicate a weak tendency for increasing NBE peak power to be associated with a decrease in the rise time of the NBE Log-RF waveform for these categories.

Similar to Fig. 9, Fig. 10 shows scatter diagrams of the peak radiated powers versus the rise time of the Log-RF waveforms for NBEs of Types
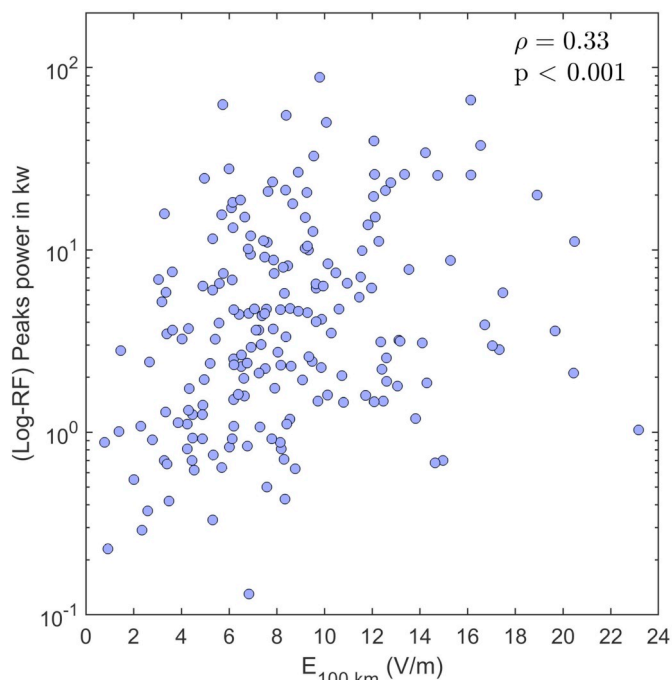
Fig. 11. Scatter plot of peak VHF power (Log-RF) versus peak FA amplitude, range normalized to 100 km, for 192 positive NBEs. ρ = Spearman correlation coefficient. p = probability value.

B-D subdivided into the INBE, Not-Isolated, and Isolated groups. These diagrams assess possible NBE power/rise time correlations within specific Type/group pairs. As with Fig. 9, the overall conclusion from Fig. 10 is that there is little or no correlation between NBE power and NBE rise time in the Log-RF waveforms. The only scatter diagram with a likely correlation is Fig. 10b with a Spearman correlation coefficient of −0.61 and a probability < .001. These Spearman values suggest that Type C NBEs in the INBE group have a weak tendency for a negative correlation between waveform rise time and peak radiated power; i.e., that NBE waveform rise time tends to decrease with increasing peak radiated power. However, the data in Fig. 10b indicate that a wide range of NBE powers can have either fast rise times (< 3 μs) or slow rise times (> 4 μs).

4.3.4. Comparison of FA E-Change data with Log-RF VHF data for positive NBEs

In the frequency bands of our sensors, the VHF radiation (Log-RF data) is dominated by short charge motions (length ~ 1.6 m) while the electric field change (FA data) is dominated by much longer charge motions (> 120 m). With combined observations for many NBEs, it is of interest to see if the peak radiated VHF power of the short charge motions is correlated with the peak E-change amplitude of the longer charge motions. (Note that peak E-change amplitude is also directly related to peak current and peak power (e.g., Krider, 1992).) Fig. 11 shows a scatter plot of Log-RF power and range normalized FA amplitude (E_{100km}) for 192 positive NBEs along with the Spearman correlation parameters. (Nine NBEs were excluded because they lacked sensor data at a range > 20 km.) Although Spearman parameters suggest a possible weak positive correlation between Log-RF power and E_{100km} amplitude, any particular Log-RF power can be found with a wide range of E_{100km} values. For example, positive NBEs with Log-RF power of ~2 kW have E_{100km} values ranging from ~2 V/m to ~17 V/m.

It is also of interest to investigate the time difference, ΔT, of the peak values of the FA and Log-RF pulses for the 201 positive NBEs. Fig. 12a and b show the ΔT peak time comparison for two NBEs. Fig. 12a shows an NBE having the FA peak precede the Log-RF peak by 0.9 μs (ΔT = +0.9 μs) while Fig. 12b shows an NBE having the FA peak

follow the Log-RF peak by 0.4 μs (ΔT = −0.4 μs). Fig. 12c shows two histograms of ΔT. The upper (red) histogram shows ΔT's > 0, that is with the FA peak preceding the Log-RF peak, while the lower (gray) histogram shows ΔT's < 0 with the FA peak following the Log-RF peak. Combining the ΔT's of both histograms, 143 (71%) of the NBEs had |ΔT| ≤ 1 μs, while only 10% of the NBEs had |ΔT| ≥ 2 μs with a maximum |ΔT| of 5.4 μs. We know of no similar comparisons for NBEs. However, Kolmasova et al. (2019), using the same sensors as used herein, studied FA and VHF (Log-RF) data for IB pulses that occurred in first 2.0 ms of 20 CG flashes in Mississippi thunderstorms. Kolmasova et al. (2019) identified 201 classic IB pulses in the 20 flashes and found that "VHF pulses systematically accompany all classical IB pulses." Furthermore, in the 20 CG flashes they studied, the percentage of "larger" IB pulse FA peaks and Log-RF pulse peaks with |ΔT| < 1 μs ranged from 38% to 91% with an average of 66%. (Therein, "larger" IB pulses satisfied the amplitude criterion for classic IB pulses.) Thus the percentage of larger IB pulses with |ΔT| < 1 μs in the 20 CG flashes studied by Kolmasova et al. (2019) was generally similar to the 71% of +NBEs with |ΔT| < 1 μs found herein. Whatever physical mechanism (s) is (are) causing the various charge motions in positive NBEs, we can conclude that these charge motions are occurring at nearly the same time across different length scales, resulting in nearly coincident pulse peaks at the different sensor frequencies.

Kostinskiy et al. (2019) proposed a series of physical mechanisms that together might explain the initial development (roughly the first 5–10 ms) of a lightning flash, including a possible physical mechanism for NBEs (since INBEs initiate some flashes). Next we briefly describe the Kostinskiy et al. (2019) NBE mechanism and then speculate on how it might account for the findings in Figs. 11 and 12.

Kostinskiy et al. (2019) hypothesized that NBEs occur when a cosmic ray extensive air shower (EAS) interacts with a large number of small thunderstorm volumes (E_{th}-volumes) where turbulent motions have enhanced the local electric field to be ≥3 MV/(m atm), which is the field needed to start a positive streamer flash in non-conducting air. (A positive streamer flash has a length of ~1 m and contains many positive streamers.) For simplicity assume that the EAS moves vertically downward through a thunderstorm. The many relativistic charged particles of the EAS pass almost simultaneously through many E_{th}-volumes at the same altitude in the cloud and start many short positive streamer flashes, which radiate strongly in the VHF and are therefore seen with our Log-RF sensors. Thus the NBE Log-RF power is proportional to the number of positive streamer flashes initiated by the EAS. Although the positive streamer flashes have velocities of only ~10^6 m/s, the relativistic EAS particles develop positive streamer flashes as a phase wave along a path 100's of meters long with an apparent motion (phase speed) of ~10^8 m/s; this longer path would easily be seen by our FA sensors. The length of the phase wave depends on the geometrical distribution of E_{th}-volumes relative to the direction of the developing EAS. Thus the FA E_{100km} amplitudes might be expected to depend more on the apparent length of overall positive streamer flash development than on the total number of positive streamer flashes in the NBE, since the FA would not detect an individual (short) positive streamer flash. We therefore speculate that the NBE Log-RF power should be only weakly correlated with the NBE FA E_{100km} amplitude, as shown in Fig. 11. Furthermore, we speculate that the peak in the NBE Log-RF power will occur with the maximum number of concurrent positive streamer flashes while the peak in the E_{100km} amplitude will occur at the time of the maximum apparent length of phase wave of positive streamer flashes. These two peak times should be roughly the same, but it should not be surprising to find, as seen in Fig. 12, that the FA peak sometimes leads and sometimes follows the Log-RF peak by a few μs or less.

5. Summary and conclusions

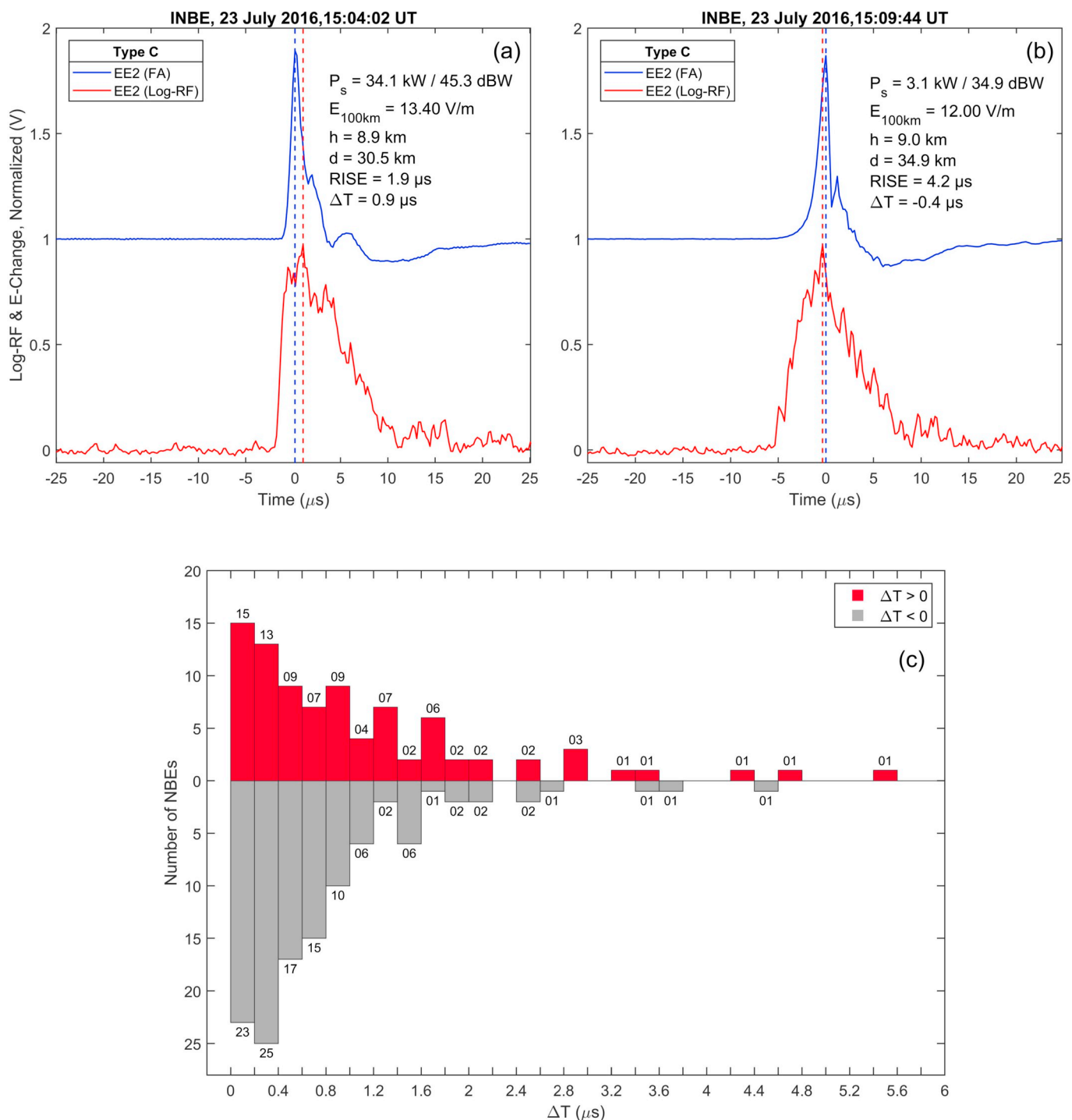In this study we analyzed 201 positive NBEs identified in Mississippi

Fig. 12. (a) +NBE (Type C + B, INBE) with vertical dashed lines showing the time difference, ΔT, between FA peak and Log-RF peak; ΔT = 0.9 μs. In this example ΔT > 0 because the Log-RF peak occurred after the FA peak. (b) Similar to (a), showing ΔT for another +NBE (Type C, INBE); ΔT = −0.4 μs and is negative because the Log-RF peak occurred before the FA peak. (c) Histograms of time difference (ΔT) between FA peak and Log-RF peak for 201 NBEs, with ΔT > 0 if the Log-RF peak occurs after the FA peak. Note that 72% of the NBEs had |ΔT| ≤ 1 μs, while only 10% of the NBEs had |ΔT| ≥ 2 μs.

thunderstorms using both fast antenna (FA) electric field change data and VHF (Log-RF) data, and we determined the NBE properties for both the FA and Log-RF waveforms. To our knowledge, this is the first time that VHF waveform properties of positive NBEs have been characterized; Bandara et al. (2019) characterized the VHF waveform properties of negative NBEs.

Using the scheme of Karunarathne et al. (2015) only 188 of the 201 NBEs could be classified as Types A through D based on their FA waveforms; most of the other 13 NBEs would fit into types 7 to 11 in the

more recent CID classification scheme of Leal et al. (2019). We also classified 146 of these 188 NBEs into three spatiotemporal groups: INBE, Not-isolated, and Isolated, according to their proximity in time and space to other lightning events (Karunarathne et al., 2015). Results of these classifications and comparisons to the prior studies in Florida are given in Tables 1 and 2. In general, we found a lower percentage of these positive NBEs were Type B and a much higher percentage were Type C compared to Karunarathne et al. (2015) using similar FA instrumentation. For the FA data we determined five NBE waveform

properties: range normalized peak amplitude (E_{100km}), rise time, FWHM (full width at half maximum amplitude), zero cross time, and duration. Resulting values are given and compared to prior work in Table 3. For the VHF (Log-RF) data we determined three NBE waveform properties: peak power, rise time, and duration.

Based on these analyses of positive NBEs in Mississippi thunderstorms, we find the following:

1. The fast antenna E-change waveform properties (Table 3) of 188 positive NBEs in Mississippi thunderstorms were in reasonable agreement with previous studies of positive NBEs, except that the few (3) Type A NBEs in this study all had small range-normalized amplitudes. For the full set of 201 positive NBEs, the average peak amplitude was 8.0 V/m range-normalized to 100 km with a standard deviation of $\pm$ 4.0 V/m (Table 3).

2. In Mississippi thunderstorms, Type B positive NBEs occurred on average at a higher altitude (12.2 km) than the other types of NBEs, while Type A NBEs were substantially lower on average (6.6 km) than the other types of NBEs (Fig. 1).

3. The maximum VHF source power of 88.4 kW for positive NBEs in Mississippi thunderstorms was substantially larger than the maximum VHF power for all three types of negative NBEs (NNBEs) in the same thunderstorms (Bandara et al., 2019): (a) high altitude NNBEs (maximum power of 7.4 kW); (b) typical, bipolar, low altitude NNBEs (maximum power of 1.3 kW); (c) low altitude, hump-type NNBEs (maximum power of 0.02 kW). Note that the dividing altitude between low and high altitude NNBEs was 8.0 km in Bandara et al. (2019).

4. Types C and D NBEs had both wider VHF peak power ranges (0.2–88.4 kW and 0.5–62.7 kW, respectively) and greater mean values (9.2 kW and 13.2 kW, respectively) than Types A and B NBEs (Fig. 7). Thus, for positive NBEs in Mississippi thunderstorms, Types C and D tend to be more energetic in the VHF than Types A and B. It should also be noted that Type C is the most common in our dataset (48%), and half of these Type C NBEs are the first event in an IC flash, that is, they are INBEs.

5. The INBE group of positive NBEs in Mississippi thunderstorms (NBEs that are the first event in an IC flash) had a larger range of VHF peak power (0.2–88.4 kW) than the range of the Not-Isolated and Isolated groups, which together was 0.1–26.7 kW (Fig. 8). The INBE group also had a larger average peak power (9.9 kW) than the Not-Isolated and Isolated Groups (4.0 and 8.7 kW, respectively). We note, however, that 53% of INBEs had peak VHF power $<$ 5 kW, so an NBE does not need to have a large source power to initiate an intracloud flash.

6. There was no systematic relationship between the peak VHF (Log-RF) powers and the rise time of the Log-RF waveform for positive NBEs (Figs. 9 and 10).

7. The bandwidths of the FA and Log-RF sensors used to study positive NBEs in this work were quite different (0–2.6 MHz versus 186–192 MHz, respectively) and imply that the sensors responded to charge motions of quite different lengths ($>$ 120 m versus 1.6 m, respectively). Despite these differences, the magnitude of the time difference, $|\Delta T|$, between the FA peak and the Log-RF peak was ≤ 1 μs for 71% and ≤ 2 μs for 90% of the 201 positive NBEs (Fig. 12). On the other hand, a comparison of the FA range-normalized peak amplitude and the Log-RF peak power for 201 positive NBEs indicated little or no correlation (Fig. 11). We offered speculations for the findings in both Figs. 11 and 12.

It is hoped that the above findings will be useful in determining the physical mechanism(s) that produce positive NBEs.

Funding

Declaration of Competing Interest

None.

Acknowledgements

References

Ahmad, N., Fernando, M., Baharudin, Z.A., Cooray, V., Ahmad, H., Abdul Malek, Z., 2010. Characteristics of narrow bipolar pulses observed in Malaysia. J. Atmos. Solar-Terrestrial Phys. 72, 534–540. https://doi.org/10.1016/j.jastp.2010.02.006.

Bandara, S., Marshall, T., Karunarathne, S., Karunarathne, N., Siedlecki, R., Stolzenburg, M., 2019. Characterizing three types of negative narrow bipolar events in thunderstorms. Atmos. Res. 227, 263–279. https://doi.org/10.1016/j.atmosres.2019.05.013.

Betz, H.-D., Marshall, T.C., Stolzenburg, M., Schmidt, K., Oettinger, W.P., Defer, E., Konarski, J., Laroche, P., Dombai, F., 2008. Detection of in-cloud lightning with VLF/LF and VHF networks for studies of the initial discharge phase. Geophys. Res. Lett. 35, L23802. https://doi.org/10.1029/2008GL035820.

Hamlin, T., Light, T.E., Shao, X.M., Eack, K.B., Harlin, J.D., 2007. Estimating lightning channel characteristics of positive narrow bipolar events using intrachannel current reflection signatures. J. Geophys. Res. Atmos. 112, 1–8. https://doi.org/10.1029/2007JD008471.

Jacobson, A.R., 2003. How do the strongest radio pulses from thunderstorms relate to lightning flashes? J. Geophys. Res. 108 (D24), 4778. https://doi.org/10.1029/2003JD003936.

Karunarathne, S., Marshall, T.C., Stolzenburg, M., Karunarathna, N., Vickers, L.E., Warner, T.A., Orville, R.E., 2013. Locating initial breakdown pulses using electric field change network. Journal of Geophysical Research Atmospheres 118 (13), 7129–7141. https://doi.org/10.1002/jgrd.50441.

Karunarathne, S., Marshall, T.C., Stolzenburg, M., Karunarathna, N., 2015. Observations of positive narrow bipolar pulses. J. Geophys. Res. 120, 7128–7143. https://doi.org/10.1002/2015JD023150.

Kolmasova, I., Marshall, T., Bandara, S., Karunarathne, S., Stolzenburg, M., Karunarathne, N., Siedlecki, R., 2019. Initial breakdown pulses accompanied by VHF pulses during negative cloud-to-ground lightning flashes. Geophysical Research Letters. https://doi.org/10.1029/2019GL082488. 2019GL082488.

Kostinskiy, A., Marshall, T., Stolzenburg, M., 2019. The Mechanism of the Origin and Development of Lightning from Initiating Event to Initial Breakdown Pulses. http://arxiv.org/abs/1906.01033.

Krider, E.P., 1992. On the electromagnetic fields, Poynting vector, and peak power radiated by lightning return strokes. J. Geophys. Res. 97 (D14), 15,913–15,917.

Le Vine, D.M., 1980. Sources of the strongest RF radiation from lightning. J. Geophys. Res. 85, 4091. https://doi.org/10.1029/JC085iC07p04091.

Leal, A.F.R., Rakov, V.A., Rocha, B.R.P., 2019. Compact intracloud discharges: New classification of field waveforms and identification by lightning locating systems. Electr. Power Syst. Res. 173, 251–262. https://doi.org/10.1016/j.epsr.2019.04.016.

Marshall, T., Bandara, S., Karunarathne, N., Karunarathne, S., Kolmasova, I., Siedlecki, R., Stolzenburg, M., 2019. A study of lightning flash initiation prior to the first initial breakdown pulse. Atmos. Res. https://doi.org/10.1016/j.atmosres.2018.10.013.

Medelius, P., Thomson, M., Pierce, S., 1991. E and DE/DT waveshapes for narrow bipolar pulses in intracloud lightning.

Nag, A., Rakov, V.A., 2010. Compact intracloud lightning discharges: 1. Mechanism of electromagnetic radiation and modeling. J. Geophys. Res. 115, D20102. https://doi.org/10.1029/2010JD014235.

Nag, A., DeCarlo, B.A., Rakov, V.A., 2009. Analysis of microsecond and sub-microsecondscale electric field pulses produced by cloud and ground lightning discharges. Atmos. Res. 91, 316.

Nag, A., Rakov, V.A., Tsalikis, D., Cramer, J.A., 2010. On phenomenology of compact intracloud lightning discharges. J. Geophys. Res. 115, D14115. https://doi.org/10.1029/2009JD012957.

Rison, W., Thomas, R.J., Krehbiel, P.R., Hamlin, T., Harlin, J., 1999. A GPS-based three-dimensional lightning mapping system: initial observations in central New Mexico. Geophys. Res. Lett. 26, 3573–3576. https://doi.org/10.1029/1999GL010856.

Rison, W., Krehbiel, P.R., Stock, M.G., Edens, H.E., Shao, X.-M., Thomas, R.J., Stanley, M.A., Zhang, Y., 2016. Observations of narrow bipolar events reveal how lightning is initiated in thunderstorms. Nat. Commun. 7, 10721. https://doi.org/10.1038/ncomms10721.

Smith, D.A., Shao, X.M., Holden, D.N., Rhodes, C.T., Brook, M., Krehbiel, P.R., Stanley, M., Rison, W., Thomas, R.J., 1999. A distinct class of isolated intracloud lightning

discharges and their associated radio emissions. J. Geophys. Res. Atmos. 104, 4189–4212. https://doi.org/10.1029/1998JD200045.

Smith, D.A., Eack, K.B., Harlin, J., Heavner, M.J., Jacobson, A.R., Massey, R.S., Shao, X.M., Wiens, K.C., 2002. The Los Alamos sferic array: a research tool for lightning investigations. J. Geophys. Res. Atmos. 107, 1–15. https://doi.org/10.1029/2001JD000502.

Smith, D.A., Heavner, M.J., Jacobson, A.R., Shao, X.M., Massey, R.S., Sheldon, R.J., Wiens, K.C., 2004. A method for determining intracloud lightning and ionospheric heights from VLF/LF electric field records. Radio Sci. 39https://doi.org/10.1029/2002RS002790. n/a-n/a.

Stolzenburg, M., Marshall, T.C., Karunarathne, S., Karunarathna, N., Orville, R.E., 2014. Leader observations during the initial breakdown stage of a lightning flash. Journal of Geophysical Research: Atmospheres 119 (21), 12,198–12,221. https://doi.org/10.1002/2014JD021994.

Thomas, R.J., Krehbiel, P.R., Rison, W., Hamlin, T., Harlin, J., Shown, D., 2001.

Observations of VHF source powers radiated by lightning. Geophys. Res. Lett. 28, 143–146. https://doi.org/10.1029/2000GL011464.

Willett, J.C., Bailey, J.C., Krider, E.P., 1989. A class of unusual lightning electric field waveforms with very strong high-frequency radiation. J. Geophys. Res. 94, 16255. https://doi.org/10.1029/JD094iD13p16255.

Wu, T., Dong, W., Zhang, Y., Wang, T., 2011. Comparison of positive and negative compact intracloud discharges. J. Geophys. Res. 116, D03111. https://doi.org/10.1029/2010JD015233.

Wu, T., Dong, W., Zhang, Y., Funaki, T., Yoshida, S., Morimoto, T., Ushio, T., Kawasaki, Z., 2012. Discharge height of lightning narrow bipolar events. J. Geophys. Res. 117, D05119. https://doi.org/10.1029/2011JD017054.

Wu, T., Yoshida, S., Ushio, T., Kawasaki, Z., Wang, D., 2014. Lightning-initiator type of narrow bipolar events and their subsequent pulse trains. J. Geophys. Res. Atmos. 119, 7425–7438. https://doi.org/10.1002/2014JD021842.